ETH IPP
Institute for Particle Physics

ETHZ-IPP Internal Report 2002-02
March 2002

Precise Energy Calibration Measurement at the SLS Storage Ring by Means of Resonant Spin Depolarization

Master Thesis of
Simon Christian Leemann

Diploma Professor
Prof. Dr. Ralph Eichler, ETHZ/PSI

Supervision
Dr. Lenny Rivkin, Dr. Michael Böge, SLS/PSI

This paper[1] is submitted as a Diploma/Master Thesis to the Institute of Particle Physics at the Swiss Federal Institute of Technology, Zurich. The work was conducted in the group of Prof. Dr. Ralph Eichler under supervision of Dres. Lenny Rivkin and Michael Böge at the Swiss Light Source SLS[2].

[1]Copies of this paper can be found online at `http://www.simonleemann.ch/work.html` or can be obtained by sending e-mail to the author at `sl@simonleemann.ch`

[2]Swiss Light Source SLS, Paul Scherrer Institute PSI, Villigen, Switzerland

Contents

1 Abstract

Due to the presence of spin flip radiation electrons get polarized anti-parallel to the main bending magnet field. Polarization values close to the Sokolov-Ternov level of 92.4% are expected for the Swiss Light Source (SLS) storage ring at 2.4 GeV. Resonant excitation at the spin precession frequency depolarizes the electron beam. This frequency happens to be proportional to the average beam energy with a factor which only depends on the g-factor of the electron. The polarization level influences the beam lifetime due to the polarization dependent Touschek scattering process. A sudden change of polarization gives rise to a change of the loss rates. Thus a fast vertical kicker magnet driven by a frequency generator and a fast loss monitor are sufficient to carry out the energy calibration measurement.

In the first part of the thesis some predictions for the anticipated polarization level as well as for the desired kicker parameters and depolarization times are made. Experiments show that polarization values well above 80% can be achieved in the SLS storage ring.

In the second part of the thesis the energy calibration experiments carried out are described involving the readout of loss monitors and the control of a frequency generator driving a fast kicker magnet. The energy calibration experiments have shown that the SLS storage ring operates at an actual beam energy of (2.4361±0.00018) GeV which is 1.5% higher than the design energy! This large discrepancy remains to be explained in further experiments.

2 Introduction

2.1 Previous Electron Beam Energy Measurements

In order to understand beam dynamics in the SLS Storage Ring it is of fundamental interest to know the precise beam energy. Once the energy is known further studies on beam energy stability over beam lifetime, energy shifts and non-linearities of the momentum compaction factor can be performed.

Until now the most precise beam energy measurements have been calibration measurements of the dipole fields in the bending magnets with Hall probes. These measurements have led to a presumed energy precision [1] of $\frac{\Delta E}{E} = (1-2) \cdot 10^{-3}$.

In order to get the beam energy with a precision better than $\frac{\Delta E}{E} = 10^{-3}$ new measures have to be taken. One possibility is to measure the resonant excitation frequency at which the spins ensemble gets resonantly depolarized [2]. This technique has recently been used successfully at ELSA [3], BESSY II [4] and ALS [5]. The next sections will discuss polarization of electron beams, depolarizing effects and will explain how the polarization level of an electron storage ring can be determined.

2.2 Polarization of Electron Beams

As first mentioned by Ternov, Loskutov and Korovina in 1961 electrons gradually polarize in storage rings due to sustained transverse acceleration while orbiting. The mechanism is the emission of *spin-flip synchrotron radiation*: While being accelerated, electrons radiate electromagnetic waves in quanta of photons which carry a spin.

Therefore two cases must be distinguished: After emitting the synchrotron photon the electron spin stays in its initial state or flips over. It has been shown [6] that only an extremely small fraction ($\sim 10^{-11}$) of the emitted power is due to spin-flip radiation, the large fraction of other synchrotron emissions has no influence on the electron's spin. Nevertheless, the process of spin-flip radiation is crucial in order to understand the meaning of *beam polarization.*

The transition rates for the two possible spin-flips have been calculated [6] [7] to be:

$$W_{\uparrow\downarrow} = \frac{5\sqrt{3}}{16} \cdot \frac{e^2 \gamma^5 \hbar}{{m_e}^2 c^2 \rho^3} \cdot \left(1 + \frac{8}{5\sqrt{3}}\right) \tag{1}$$

$$W_{\downarrow\uparrow} = \frac{5\sqrt{3}}{16} \cdot \frac{e^2\gamma^5\hbar}{{m_e}^2c^2\rho^3} \cdot \left(1 - \frac{8}{5\sqrt{3}}\right) \tag{2}$$

where γ is the Lorentz factor and ρ is the instantaneous bending radius. The symbol $\uparrow$ denotes the spin along the guiding dipole field, whereas the symbol $\downarrow$ denotes a spin against the guiding dipole field.

The difference between these two rates causes an injected electron beam to get *polarized* anti-parallel with respect to the guiding dipole field (for positrons the accumulated polarization would be along the guiding dipole field). The maximum achievable polarization level in a planar ring without imperfections is given by:

$$P_{ST} = \frac{W_{\uparrow\downarrow} - W_{\downarrow\uparrow}}{W_{\uparrow\downarrow} + W_{\downarrow\uparrow}} = \frac{8}{5\sqrt{3}} = 92.38\% \tag{3}$$

where P_{ST} is the *Sokolov-Ternov Level* of polarization [8]. The time constant of the exponential build-up process of this *equilibrium polarization* by the initially unpolarized beam is:

$$\tau_p = (W_{\uparrow\downarrow} + W_{\downarrow\uparrow})^{-1} = \left(\frac{5\sqrt{3}}{8} \cdot \frac{e^2\hbar}{{m_e}^2c^2}\right)^{-1} \cdot \frac{\rho^3}{\gamma^5} \tag{4}$$

In case of the SLS storage ring τ_p is roughly 31 minutes. So finally, we would expect *polarization build-up* to be described by:

$$P(t) = P_{ST}\left(1 - \exp\left(-\frac{t}{\tau_p}\right)\right) \tag{5}$$

Meaning that an unpolarized beam can be injected into the SLS storage ring and after roughly an hour over 85% of the beam will be fully polarized anti-parallel to the guiding dipole field!

However we have (until now) neglected diffusion effects on spin orientation. Similar to the fact that radiation damping does not lead to dimensionless beam size due to quantum emission, spin-flip radiation is accompanied by the depolarizing effect of *spin diffusion*. Thus the measured beam polarization is an equilibrium state and shall be examined in the next chapters.

2.3 Spin Dynamics

The electron spin interacts with the electromagnetic field through the magnetic moment associated with the spin:

$$\vec{\mu} = \frac{ge}{2m_e c}\hbar\vec{S} \tag{6}$$

where g is the gyromagnetic ratio of the electron . The deviation of this value from 2 is the *anomalous magnetic moment* of the electron:

$$a = \frac{g-2}{2} = 0.00115965 \tag{7}$$

We consider an electron at rest in a magnetic field $\vec{B}$; the precession equation of motion for the spin is the Larmor equation:

$$\frac{d\vec{S}}{dt} = \vec{\Omega} \times \vec{S} \tag{8}$$

with the angular velocity

$$\vec{\Omega} = -\frac{ge}{2m_e c}\vec{B} \tag{9}$$

Using Lorentz transformations the last equations can be rewritten [6] for a relativistic electron moving in the electromagnetic field $\vec{E}$ and $\vec{B}$ in an accelerator:

$$\vec{\Omega}_{lab} = -\frac{e}{m_e c}\left[\left(a+\frac{1}{\gamma}\right)\vec{B} - \frac{a\gamma}{\gamma+1}\vec{\beta}\left(\vec{\beta}\cdot\vec{B}\right) - \left(a+\frac{1}{\gamma+1}\right)\vec{\beta}\times\vec{E}\right] \tag{10}$$

which, when substituted into equation 8 (where $\vec{S}$ is in the rest frame of the electron) is called the *Thomas-BMT Equation* where BMT stands for Bargman, Michel, Telegdi [9].

In a storage ring like SLS several types of fields are applied to the electron and are seen by the circulating particle periodically with period $2\pi R$, therefore it is more convenient to change the time variable t into the traveled distance of the electron $s = \beta ct$. Most of the applied fields (quadrupole or sextupole magnets) only have an effect on an electron's orbit if its trajectory deviates from the designed circular orbit. The ideal electron traveling along the designed orbit will only see the guiding magnetic dipole field with $\vec{B}(s) = \vec{B}(s + 2\pi R)$ as well as the accelerating electric field $\vec{E}$. The accelerating field however, does not cause spin precession on the ideal electron because $\vec{E} \parallel \vec{\beta}$. So we finally derive the spin precession of a highly relativistic ($\frac{1}{\gamma} \ll 1$) electron to be:

$$\frac{d\vec{S}}{ds} = -\frac{e}{m_e c\gamma} \Big((1+a)\,\vec{B}_{\parallel} + (1+a\gamma)\,\vec{B}_{\perp} \Big) \times \vec{S} \tag{11}$$

where $\vec{B}_{\parallel}$ and $\vec{B}_{\perp}$ are the magnetic fields parallel and perpendicular to the trajectory. In a flat machine (like SLS) the ideal electron sees $\vec{B}_{\perp} \parallel \vec{e}_z$ (leading to Thomas precession) and vanishing $\vec{B}_{\parallel}$ (leading to Larmor precession) [10] [11]. We now are able to write the spin precession frequency in the particle's rest frame (i.e. in machine coordinates):

$$\vec{\Omega}_{sp} = \frac{e\vec{B}_{\perp}}{m_e c\gamma} \cdot a\gamma \tag{12}$$

with the relativistic cyclotron frequency (the revolution frequency of the particles in the storage ring)

$$\omega_0 = \frac{e\vec{B}_{\perp}}{m_e c\gamma} \tag{13}$$

and the *spin tune*

$$\nu = a\gamma \tag{14}$$

describing the number of times the spin vector precesses around the bending field vector for one turn of the particle around the ring. This is shown schematically in Figure 1. The relationship between spin precession frequency and energy of the particles (equation 12) is the mechanism which is used to determine the precise energy of the electrons in the SLS storage ring (see chapter 3.1).

A solution to equations 11 and 12 for the flat machine therefore leads to $\vec{S}_z$ (the component of the spin in direction of the main bending field $\vec{B}_{\perp}$) remaining constant. The other components $\vec{S}_x, \vec{S}_y$ are statistically distributed among the electrons in the beam. After integration over all the electrons in the ensemble the only remaining component is $\vec{S}_z$. The time-integration of the remaining component over the ensemble leads to a constant degree of polarization.

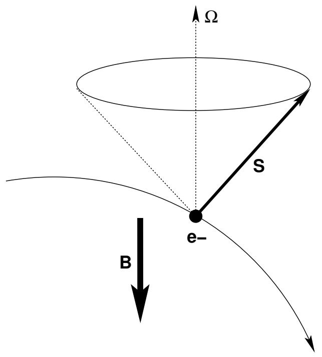

Figure 1: *Precession of the electron spin around the main bending magnet field.*

2.4 Depolarizing Effects

In a real storage ring like SLS electrons oscillate around a certain trajectory which is repeated during every revolution, the so called *closed orbit*. The closed orbit is determined among others by radial field errors (*vertical closed orbit*) and vertical field errors (*horizontal closed orbit*) as well as misaligned quadrupoles and sextupoles — these errors cause the closed orbit to go through the elements off-centered. An electron not on the closed orbit (deviations in the order of $\sim \mu m$ from the closed orbit) will perform *betatron oscillations* around it; this motion is however damped by synchrotron radiation. Because the electrons do not necessarily pass quadrupole or sextupole magnets in their center, they see perpendicular fields in addition to the main bending field. Furthermore the electrons see the time-varying fields of kicker and corrector magnets as well as possible errors like misalignment of magnets or dipole rolls (i.e. when a dipole magnet's misalignment is a rotation around the design orbit). All these additional field components have to be considered in equation 11.

Longitudinal magnetic fields (found in insertion devices and in case of dipole pitch, i.e. when a dipole is aligned out of the horizontal plane) lead to Larmor precession of the spin around the electron's momentum axis resulting in a change of $\vec{S}_z$. Radial magnetic fields (found in quadrupoles, sextupoles and vertical kicker magnets as well as in case of dipole rolls) lead to Thomas precession perpendicular to the electron's momentum axis, which again results in a change of $\vec{S}_z$ (see figure 2).

If these additional fields in conjunction with spin diffusion result in $\vec{S}_z = 0$

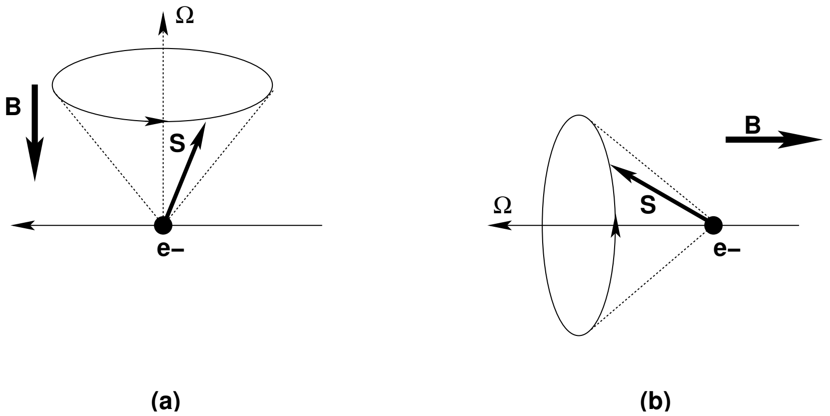

Figure 2a: *Thomas Precession.* Figure 2b: *Larmor Precession*

we refer to a *depolarized beam* which has a polarization degree of zero[3]. The important difference between depolarizing effects is their energy dependency. As shown in equation 11 precession due to longitudinal fields depend inversely on the energy whereas radial and vertical fields lead to energy independent precession; therefore in high energy machines the longitudinal field effects can be neglected when compared to transverse fields.[4]

In order to depolarize the beam at SLS (flat machine) radial fields are needed. Applying the field from a time-varying vertical kicker magnet, the spin's precession cone angle is enlarged from 0 towards $\frac{\pi}{2}$. Together with the effect of *spin diffusion* this leads to the point where $\vec{S}_z = 0$ when integrating over many electrons therefore resulting in zero polarization (see figure 3).

Assume a vertical kicker magnet applying to the electrons in the storage ring

[3]This refers to a simple model. Actually one should find a periodic solution of the Thomas-BMT equation by integrating around the periodic closed orbit. Similar to the fact that horizontal and vertical displacements from the design orbit lead to a periodic solution for the orbital motion (the closed orbit) there is a periodic solution of the Thomas-BMT equation on the closed orbit for the spin vector $\vec{n}_0$ which obeys $\vec{n}_0(s+L) = \vec{n}_0(s)$. This more detailed approach shows that in a perfectly flat machine $\vec{n}_0 \parallel \vec{B}_\perp \parallel \vec{e}_z$ but in real machines $\vec{n}_0$ has slight deviations from $\vec{B}_\perp$ which in fact determines the equilibrium polarization level. [10]

[4]However one must keep in mind that in storage rings typical field errors (from magnet misalignment for example) are proportional to the beam energy E, i.e. after passing through an error field the electron's angular deflection is independent of E. Yet for the spin the dependency is different: The spin vector is perturbed by an angle $a\gamma\theta$ which is proportional to E. Hence the higher the beam energy, the more sensitive the electrons are to errors and therefore the more vulnerable the beam is to depolarizing effects. This is well demonstrated when comparing typical levels of polarization at LEP (11% at 50 GeV) and at SPEAR (90% at 3.7 GeV). [12]

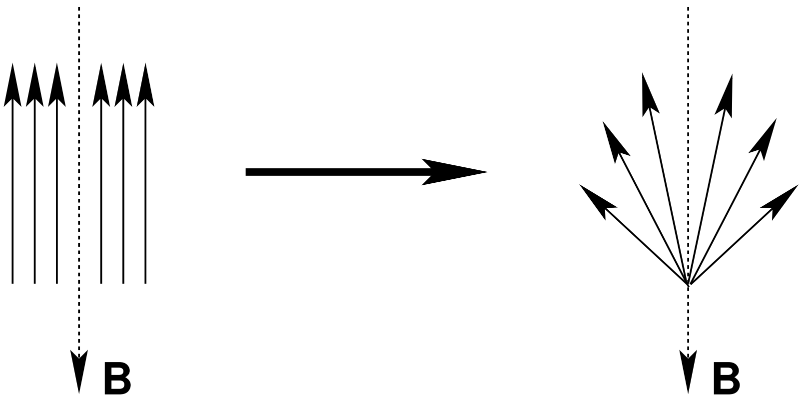

Figure 3: *The Spin diffusion process.*

a radial magnetic field $\vec{B}_{kick}$. The precession frequency along the electron's momentum direction according to equations 11, 12 is given by:

$$\vec{\Omega} = -\frac{e\vec{B}_{kick}}{m_e c} \cdot a \tag{15}$$

This process is energy independent as already mentioned. But this kicker magnet's time varying magnetic field not only has an influence on the electron's spin, but also on the trajectory of the electrons. When passing the kicker magnet the electrons are "kicked" vertically from their trajectory and a betatron oscillation around the closed orbit is excited. Normally the betatron frequency is far enough away from the chosen kicker frequency, so no resonance conditions are fulfilled; therefore the beam's deviation from the closed orbit remains very small. Nevertheless the electrons will continue on their trajectory around the ring and pass a quadrupole magnet where their displacement from the closed orbit can lead to a modification of the depolarizing effects induced by the kicker magnet.

While passing the kicker magnet the electron obeys to the simple equation (see equation 12)

$$\frac{d\vec{S}}{ds} = \vec{\Omega}_{sp} \times \vec{S} = \vec{S} \times \begin{pmatrix} 0 \\ \frac{eB_{kick}}{m_e c} \cdot a \\ 0 \end{pmatrix} \tag{16}$$

which has the solution [13]

$$\vec{S} = \begin{pmatrix} \sqrt{1 - {S_y}^2} \cdot \sin(\frac{ea}{m_e c} B_{kick} \cdot s + \vartheta) \\ \\ S_y = \mathrm{const} \\ \\ \sqrt{1 - {S_y}^2} \cdot \cos(\frac{ea}{m_e c} B_{kick} \cdot s + \vartheta) \end{pmatrix} \tag{17}$$

When the electron passes the depolarizing kicker its spin precession cone angle is widened by:

$$\Delta\theta = \frac{ea}{m_e c} \cdot (B_{kick} \cdot l) \tag{18}$$

where l is the length of the kicker. The kicker magnet actually kicks according to a sinusoidal waveform so we have to take in account that the real kicker strength is a time averaged value:

$$\overline{B_{kick}} = \frac{2}{\pi} \, B_{kick} \tag{19}$$

and therefore the actual widening in the kicker (per revolution) is:

$$\overline{\Delta\theta} = \frac{2}{\pi} \, \frac{ea}{m_e c} \cdot (B_{kick} \cdot l) \tag{20}$$

2.5 Resonant Depolarization

Using a very strong kicker magnet the spin ensemble could be tilted into the horizontal plane during one pass through the kicker field, but without spin diffusion this does not lead to beam depolarization. However over many revolutions around the ring it is possible to tilt the mean spin vector bit by bit to the horizontal plane by using time-varying magnetic fields in *resonance* with the electron's spin revolutions. This procedure is depicted in figure 4.

Recalling equation 20 we can calculate the opening angle of the precession cone after n revolutions:

$$\theta = n \cdot \overline{\Delta\theta} \tag{21}$$

and since we know that depolarization is reached by tilting the mean spin vector into the horizontal plane (over a time which is long enough to allow spin diffusion), we can define the *depolarization time* τ_{depol}:

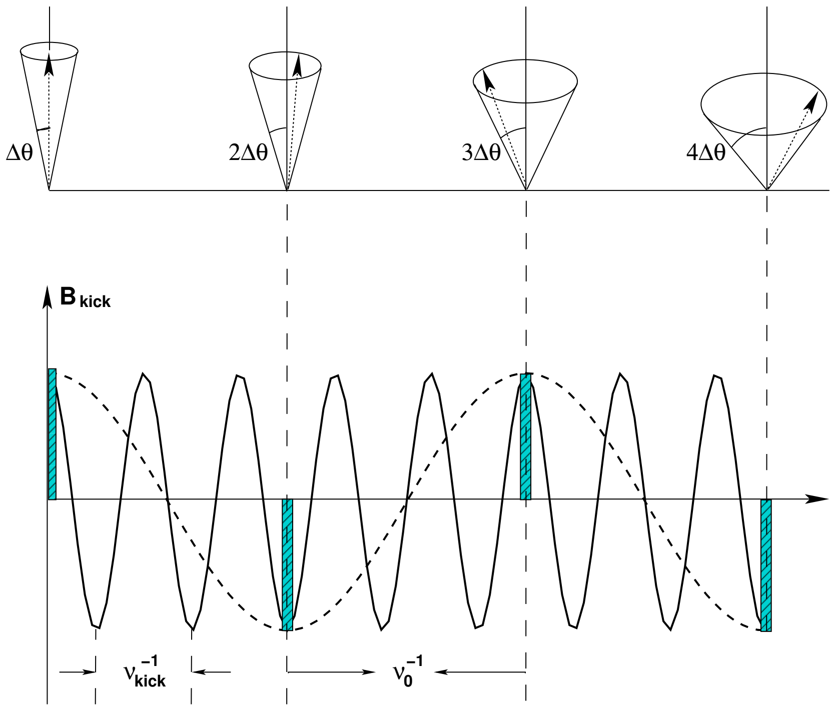

Figure 4: *For illustration: Resonant widening (half-integer resonance) of the precession cone by a time-varying magnetic kicker field. Because the electron is in this field only for a very short time (grey boxes) there are several resonant frequencies (depicted by the solid and dashed curves).* ${\nu_0}^{-1}$ *stands for the electron's revolution period around the ring, while* ${\nu_{kick}}^{-1}$ *is the period of the kicker magnet strength. [13]*

$$
\begin{aligned}
\theta &= n \cdot \overline{\Delta\theta} \\
&= n \cdot \left[\frac{2}{\pi} \frac{ea}{m_e c} \cdot (B_{kick} \cdot l)\right] \\
&= \tau_{depol} \cdot \nu_0 \cdot \left[\frac{2}{\pi} \frac{ea}{m_e c} \cdot (B_{kick} \cdot l)\right] \\
&\overset{!}{=} \frac{\pi}{2}
\end{aligned}
\tag{22}
$$

and therefore, we derive:

$$
\tau_{depol} = \frac{\pi}{2} \cdot \left[\frac{2}{\pi} \frac{ea}{m_e c} \cdot (B_{kick} \cdot l)\right]^{-1} \cdot \frac{1}{\nu_0} \tag{23}
$$

In the case of the SLS storage ring this leads to:

$$
\tau_{depol}\,[s] \approx 3.48 \cdot 10^{-6} \cdot \frac{1}{B_{kick} \cdot l\,[Tm]} \tag{24}
$$

If we require depolarization time not to be longer than a second it can be derived from equation 24:

$$
B_{kick} \cdot l \geq 3.48 \cdot 10^{-6}\ T \cdot m \tag{25}
$$

Such values can be well achieved with the multi-bunch feedback kicker magnets installed at SLS ($B \cdot l < 10^{-4}\ T \cdot m$).

2.6 Beam Excitation and Resonances

As already mentioned in chapter 2.3 there is a relationship between spin motion and orbital motion; this shall be examined in this section. Assume an electron performing vertical betatron oscillations according to Hill's Equation and consider these oscillations damped weakly:

$$
\frac{d^2 z}{dt^2} + \delta \frac{dz}{dt} + {\omega_{\beta,z}}^2 z = 0 \tag{26}
$$

where δ is the damping constant and $\omega_{\beta,z}$ is the vertical betatron oscillation frequency. Now a vertical kicker magnet shall be used to excite the beam. Compared to the perturbation of the beam through the kicker magnet damping is negligible:

$$\frac{d^2z}{dt^2} + {\omega_{\beta,z}}^2 z = F(t) \tag{27}$$

The radial field $F(t)$ is time dependent, but it is more complicated than simply $\propto \cos(2\pi\nu_{kick}t)$ because the electron only sees the excitation during the small period of time in which it travels through the kicker magnet. Therefore $F(t)$ can be arranged as a cosine multiplied with a step function [13]:

$$F(t) = \left[a_0 + \sum_{n=1}^{\infty} a_n \cos(n2\pi\omega_0 t)\right] \cdot \cos(2\pi\omega_{kick}t) \tag{28}$$

where ω_0 is the revolution frequency. The solution to equation 27 is:

$$z(t) = \sum_{n=0}^{\infty} A_n \cos\left[2\pi(\omega_{kick} \pm n\omega_0)\right] \tag{29}$$

and the amplitudes are determined by:

$$A_n \propto \frac{1}{{\omega_{\beta,z}}^2 - (2\pi\omega_{kick} \pm n2\pi\omega_0)^2} \tag{30}$$

The resonance condition leads to:

$$\omega_{res} = \mid \frac{\omega_{\beta,z}}{2\pi\omega_0} \mp n \mid \cdot\omega_0 = \mid Q_z \mp n \mid \omega_0 \qquad n = 0, 1, 2, ... \tag{31}$$

(where Q_z is the *vertical tune*) which means that if $\omega_{kick} = \omega_{res}$ the vertical beam oscillations will be excited to a point where the beam is lost. The same can be shown for the horizontal betatron oscillations (Q_x) as well as for synchrotron motion (Q_s). Such resonances must be avoided during the whole experiment.

The motion of the spin vector can be described in a very similar way: A solution to the Thomas-BMT equation (equation 11) is given by (neglecting phase)[5]:

[5] Keep in mind that in equation 11 the spin vector $\vec{S}(s)$ was a function of the traveled distance of the electron whereas here it is a function of time $\vec{S}(t)$ which is more practical since a time-dependent field $F(t)$ has been taken into account. Notice also that equation 12 presented solutions for the spin motion in the electron's rest frame; the solutions here are in the lab frame which is the frame of interest when describing spin motion under influence of a kicker magnet field.

$$S_y(t) = A\sin(\Omega t) \qquad \text{where} \qquad A = \sqrt{1 - {S_z}^2} \ll 1 \tag{32}$$

Now the spin precession is excited with the kicker magnet:

$$\frac{d^2 S_y}{dt^2} + \Omega^2 S_y = F(t) \tag{33}$$

Taking into account again that $F(t)$ is not a pure cosine, but a cosine multiplied with a step function, one derives:

$$S_y(t) = \sum_{n=0}^{\infty} A_n \cos\left[2\pi(\omega_{kick} \pm n\omega_0)\right] \tag{34}$$

$$A_n \propto \frac{1}{\Omega^2 - (2\pi\omega_{kick} \pm n2\pi\omega_0)^2} \tag{35}$$

Keeping in mind equations 11, 12 and 14 an recalling that

$$\Omega = 2\pi\omega_0(a\gamma + 1) \tag{36}$$

the resonant depolarizing frequencies are derived:

$$\omega_{depol} = \mid a\gamma + 1 \mp n \mid \omega_0 \qquad n = 0, 1, 2, ... \tag{37}$$

This shows that the resonant depolarizer frequencies are sidebands of the revolution frequency. The case where $n = a\gamma$ is called the *integer spin tune*. If the kicker frequency is in resonance with the depolarizing frequency ($\omega_{kick} = \omega_{depol}$) it is possible to tilt the mean spin vector of the electrons in the beam into the horizontal plane; in presence of spin diffusion effects (with a decoherence time much smaller than τ_{depol}) this depolarizes the beam.

2.7 A Polarization Model for the SLS Storage Ring

In chapter 2.2 it was shown that due to synchrotron radiation an electron beam in a storage ring will polarize with a certain characteristic time constant τ_0 to the maximum level of polarization P_{ST}. In chapter 2.4 depolarizing mechanisms were introduced. It was also mentioned that field errors had less influence on the level of polarization in low-energy machines like SLS, thus high polarization levels should be achievable at SLS. In this section a simple model for the equilibrium polarization build-up at SLS will be discussed.

Polarization build-up at SLS is described by equation 5:

$$P_{pol}(t) = P_{ST}\left(1 - \exp\left(-\frac{t}{\tau_p}\right)\right) \tag{38}$$

with $\tau_p = 1865$ s at the nominal energy of 2.4 GeV. Depolarizing effects are expected to show an exponential decay of the polarization:

$$P_{depol}(t) = P_{ST}\exp\left(-\frac{t}{\tau_d}\right) \tag{39}$$

The equilibrium state between the polarization build-up due to spin-flip radiation and depolarizing effects due to photon emission is described again by an exponential build-up:

$$P_{tot}(t) = P_{eff}\left(1 - \exp\left(-\frac{t}{\tau_{eff}}\right)\right) \tag{40}$$

where

$$P_{eff} = P_{ST}\frac{\tau_d}{\tau_p + \tau_d} \qquad \text{and} \qquad \frac{1}{\tau_{eff}} = \frac{1}{\tau_p} + \frac{1}{\tau_d} \tag{41}$$

Expecting an equilibrium polarization level of 80% at SLS one can derive the characteristic depolarization time as well as the equilibrium polarization build-up time from equation 41. In the example shown in figure 5 the following values have been used:

$$\begin{aligned} \tau_p &= 1865\ s \\ P_{eff} &\approx 80\% \\ \Longrightarrow \tau_d &\approx 12032\ s \\ \Longrightarrow \tau_{eff} &\approx 1615\ s \end{aligned}$$

It is important to note that depolarizing effects have a very long characteristic time τ_d compared to polarization build-up τ_p (in this situation) leading to high polarization values.

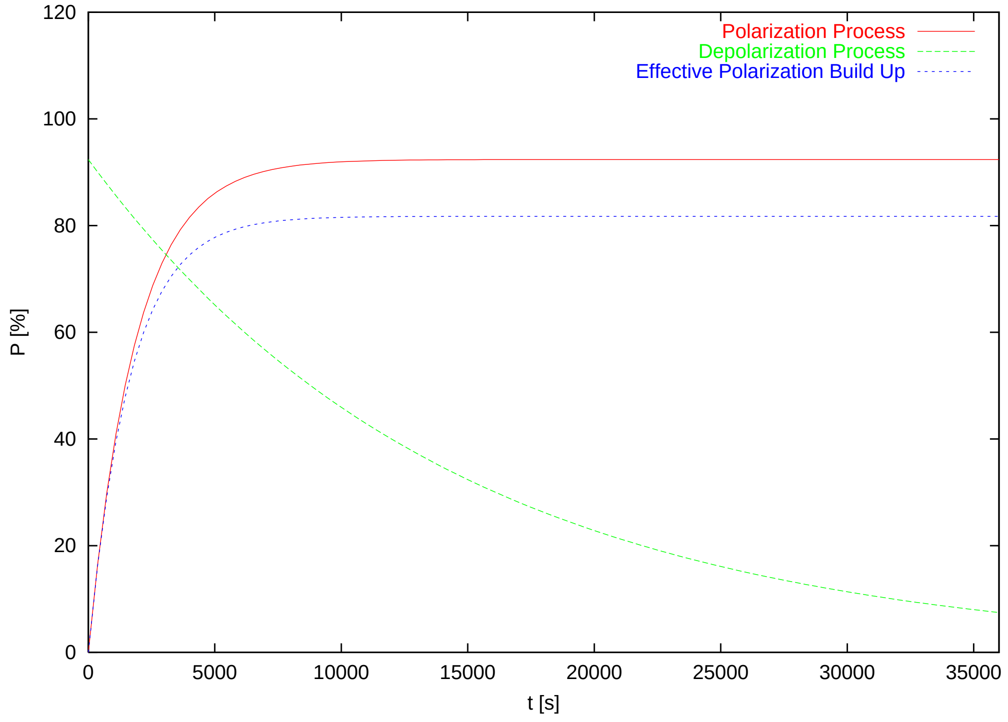

Figure 5: *A model for the effective polarization build-up in the SLS storage ring. The time interval shown is ten hours which corresponds to typical beam lifetimes.*

3 Experimental Approach and Equipment

3.1 Touschek Scattering and Polarization

Until now polarization of the electron beam as well as depolarization have been mentioned. Measuring *absolute polarization* however is not a simple task and requires dedicated complex hardware (Compton Polarimeter, dedicated beam line, etc.) which currently do not exist at SLS. But it is actually not necessary to measure absolute polarization in order to obtain the degree of equilibrium polarization. If a Touschek limited beam is used the degree of equilibrium polarization can be determined by observing the rate of Touschek scattering because Touschek scattering is *polarization-dependent*.

The three main effects which contribute to scattering of beam electrons in a storage ring are: Touschek Scattering (τ_{ts}), elastic scattering (τ_{el}) and bremsstrahlung (τ_{bs}); these effects determine beam lifetime in the SLS storage ring [14]:

$$\frac{1}{\tau} = \frac{1}{\tau_{ts}} + \frac{1}{\tau_{el}} + \frac{1}{\tau_{bs}} \tag{42}$$

Recent experiments [14] have shown τ_{bs} to be so large, that it has no significant influence on the total lifetime τ. For single bunch beam current of $0.5 - 1.5\ mA$ the dominant effect [14] is Touschek scattering; elastic scattering depends inversely on gas pressure, which in turn depends linearly on beam current. Therefore we chose to use a filling pattern of 90 bunches at about 100 mA which guarantees for Touschek limitation of the beam where:

$$\frac{1}{\tau_{ts}} \gg \frac{1}{\tau_{el}} + \frac{1}{\tau_{bs}} \tag{43}$$

Touschek scattering [15] [16] has a polarization dependent cross section:

$$\sigma_{ts} = f_1(r_e, \beta, \Theta) - P^2 \cdot f_2(r_e, \beta, \Theta, \Phi) \tag{44}$$

where f_i are functions of the electron radius r_e, the relativistic velocity β and the scattering angles Θ and Φ. Increasing beam polarization P leads to a smaller Touschek cross section and therefore to less losses of beam particles. On the other hand, a sudden decrease in beam polarization (due to the depolarizing resonance for example) will lead to a rise of Touschek scattering losses. Therefore the change of the Touschek loss rates of the beam can be correlated with changes in the polarization level.

Furthermore, measurement of the equilibrium polarization build-up time will allow determination of the equilibrium degree of polarization nevertheless: Recall equation 40 describing this build-up process. If we observe the exponential build-up the remaining unknown (τ_p can be calculated, see equation 4) τ_d can be fitted. With equation 41 the equilibrium polarization level P_{eff} can be obtained[6].

3.2 Measurands

The remaining obstacle is measuring the rate of Touschek scattering. There are three obvious ways to do this: Measure the current of the beam (its derivative is the loss rate), use scintillation monitors which register a pair of Touschek scattered electrons outside of the vacuum chamber or measure the beam intensity by analyzing the signal from the beam position monitors (BPMs). The former methods were used in our experiments. The beam current and lifetime were used to monitor the change of Touschek losses and the scintillation counters were used to monitor loss rates of Touschek scattered electron pairs.

3.2.1 Beam Current and Lifetime

Beam current and beam lifetime can both be monitored through the SLS control system. When injection into the storage ring stops the beam current slowly decays following an exponential function with a characteristic decay time:

$$I = I_0 \exp(-\frac{t}{\tau}) \qquad \text{and} \qquad \dot{I} = -I\frac{1}{\tau} \tag{45}$$

The beam lifetime is the inverse negative of the current derivative $-\dot{I}^{-1}$ and therefore the product of beam lifetime and beam current is the decay constant:

$$\tau = -\dot{I}^{-1} \cdot I \tag{46}$$

After stopping the injection one would expect a gradual decay of the current and respectively an increase in lifetime. Instead an exponential increase of

[6] Note that this is only possible for the equilibrium level. Using this method it is not possible to measure the degree of polarization at any given time, i.e. outside of the equilibrium state. This would still require a polarimeter.

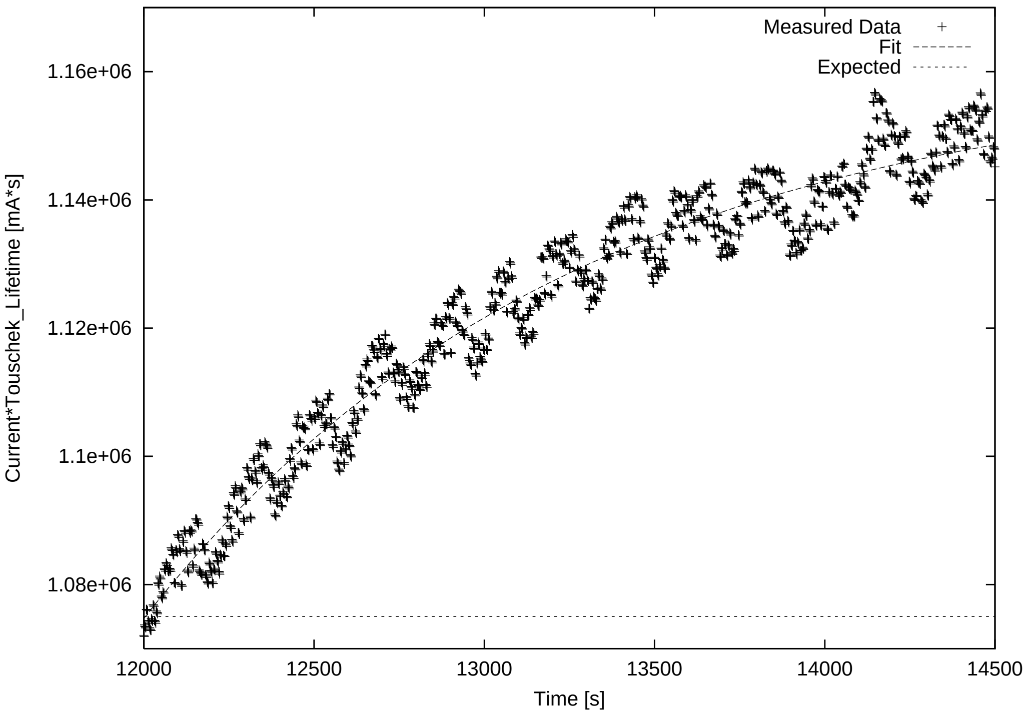

Figure 6: *The polarization build-up after injection is clearly seen in this plot. Injection stopped shortly before timestamp 12000. The fit is depicted by the dashed line. The build-up time constant is* $\tau_{ts} = (1261 \pm 12)s$ *corresponding to an equilibrium polarization degree* $P_{eff} = (62.5 \pm 0.6)\%$.

this product is observed due to the fact that Touschek scattering decreases with increasing polarization (figure 6). Recall that the characteristic decay time of the beam current in the SLS storage ring is given by:

$$\frac{1}{\tau} = \frac{1}{\tau_{ts}} + \frac{1}{\tau_{el}} \tag{47}$$

If the current is known τ_{el} can be calculated [14] and thus we derive τ_{ts}:

$$\tau_{ts} = \frac{\tau \cdot \tau_{el}}{\tau_{el} - \tau} \tag{48}$$

It was observed that after waiting for two to three polarization build-up times to pass, τ_{ts} reaches a constant value, precisely as expected from theory.

After the build-up of τ_{ts} has been observed and the stored beam has reached equilibrium state τ_{ts} stays constant. This changes when the beam is excited

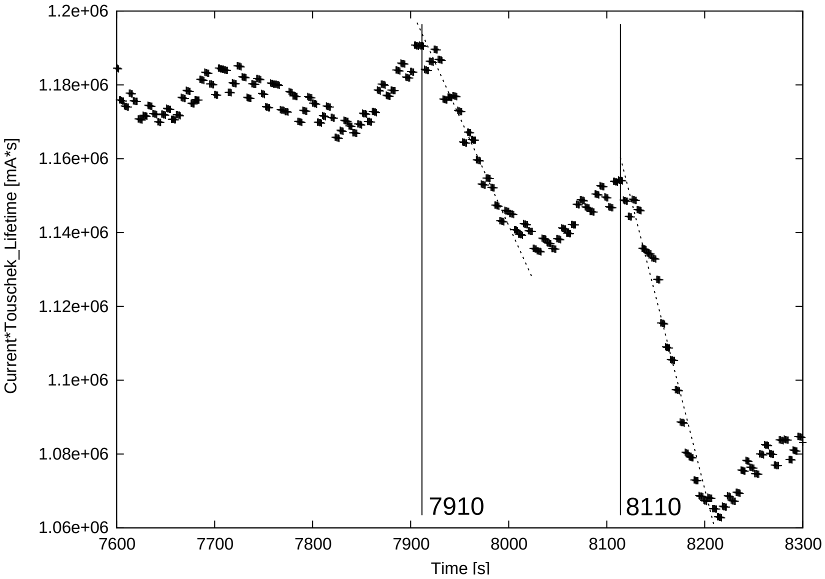

Figure 7: *The beam is excited shortly at the depolarizing resonance at timestamp 7910 and again later at timestamp 8110 leading to sudden drops in the product of beam current and lifetime.*

at the spin tune: The effective polarization is reduced and thus the Touschek scattering cross section rises leading to a decrease of beam lifetime (figure 7).

3.2.2 Loss Monitors

When the Touschek scattering rate suddenly rises because of resonant depolarization, an increase of scattered electron pairs should be detected outside the vacuum chamber. At the SLS storage ring a pair of scintillators was already installed downstream of the in-vacuum undulator U24. The closed gap of this undulator reduces the aperture to 8 mm in the straight section which leads to an increase of the signal intensity of the loss monitors. When the scintillators registered an event in coincidence we assume this a Touschek scattering event. During stable beam conditions this loss signal is constant. As soon as the beam is excited at the resonant depolarizing frequency the signal jumps to higher values. This is a very useful method to distinguish jitter of the lifetime and current readings (see figures 6 and 7) from "real" peaks. An example is given in figure 8 where the loss monitor jump clearly identifies the sudden increase of Touschek loss rates.

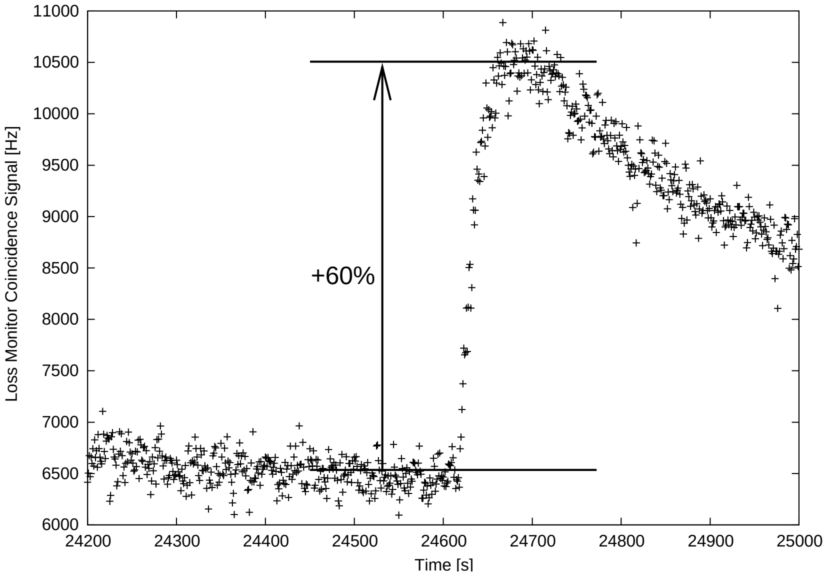

Figure 8: *Excitation of the beam at the resonant depolarizing frequency leading to a jump in the rate of Touschek scattered particles as seen by scintillation monitors.*

3.3 Finding the Depolarizing Resonance

The high precision of this resonant depolarization experiment is based on the fact that the energy measurement is actually a frequency measurement. Frequency measurements are simple, quick and very precise. Recall equation 14 describing the spin tune:

$$\nu = a\gamma = a\frac{E}{m_e c^2} \tag{49}$$

The design energy of the SLS storage ring is 2.4 GeV which leads to an estimated spin tune of $\nu = 5.4465$. The resonant depolarizing frequency is the fractional part of the spin tune multiplied with the revolution frequency:

$$\omega_{depol} = (\nu - \lfloor \nu \rfloor) \cdot \omega_0 \approx 465.1 \ kHz \tag{50}$$

So we expect to find the resonant depolarizing frequency around 465 kHz. Form this one is able to calculate the energy:

$$E = m_e c^2 \cdot \frac{1}{a} \cdot \nu = m_e c^2 \cdot \frac{1}{a} \cdot \left(\frac{\omega_{depol}}{\omega_0} + 5\right) \tag{51}$$

The resonance is found by means of sweeping over a frequency range around the expected value determining the precise frequency at which the beam gets depolarized.

This is done by using a signal generator which feeds a sine wave to the input of the kicker magnet amplifier. The frequency of this sine wave is swept over a pre-defined interval with a certain sweep velocity or *dwell* (the time span in which a sine wave of a certain frequency is fed to the amplifier). For example we could start at 400 kHz and sweep until we reach 500 kHz with a step size of 1 Hz and a dwell of 1 s meaning that upon triggering the sweep the signal generator will feed a sine wave with 400 kHz frequency to the amplifier and will raise this value linearly by one Hertz per second until it reaches 500 kHz[7]. Observing when the resonant depolarization of the beam occurs the actual frequency is recorded and the beam energy calculated according to equation 51.

Since we are using very low frequencies (the signal generator supports frequencies up to 1.1 Ghz) and we only make use of large dwells (the signal generator is capable of ms dwells) the generator is very precise; measurements of the generator output on an oscilloscope showed that the generator fed exactly the required frequency to the amplifier with a precision much higher than 1 $\frac{Hz}{s}$. It is important to note here that the uncertainty of the frequency generator's output frequency has a negligible influence on the uncertainty of this measurement because the frequency uncertainty is magnitudes smaller than other effects; these will be discussed later.

3.4 Resonance Mirror

In the last chapter we mentioned the fact that only the fractional part of the spin tune is measurable. Similar to the fact that a traveler going $\frac{3\pi}{2}$ around a circle ends at the same spot his fellow does when going around $\frac{\pi}{2}$ in the other direction, we can't be a priori sure when observing a "resonant" frequency that this isn't just the mirror frequency of the resonance. According to the Nyquist Theorem we can only measure how much below or above we are from the half-integer, but not on which side or in mathematical terms, does the

[7]Note that the mentioned sweep would require almost 28 hours while a machine shift at SLS is only 8 hours! Therefore we normally first swept at high speeds over a large interval; when a resonance is found the sweeping interval is narrowed and the sweep speed lowered to increase resolution. This is an iterative and more efficient procedure but still a very time consuming task. Once we depolarized the beam at the resonant frequency we had to wait for polarization to build up in the beam again before we could start the next sweep. Remember that the characteristic polarization time at SLS is more than a half hour!

measured frequency correspond to $\nu - \lfloor \nu \rfloor$ or $\nu + 1 - \lfloor \nu \rfloor$. For example the frequency 500 kHz corresponds to a beam energy of 2.372 GeV but also to the mirror energy at 2.475 GeV; this ambiguity is resolved in the following way:

The energy of the beam can be slightly varied using a different RF main frequency. At SLS the RF main frequency is 500 MHz. Beam energy and RF main frequency are related by the momentum compaction factor α:

$$\frac{\Delta E}{E} = -\frac{1}{\alpha} \frac{\Delta \nu_{RF}}{\nu_{RF}} \tag{52}$$

Therefore a change in the RF main frequency will lead to a change in beam energy. If the RF main frequency is changed to a lower value, the beam energy will rise. If the resonant frequency increases as well it is the "real" resonance; if however the resonant frequency decreases, it is the mirror resonance and vice-versa. Thus this procedure always requires a second measurement of the resonant frequency.

3.5 Sidebands

Energy oscillations of electrons in the beam (synchrotron oscillations) lead to a modulation of the spin tune and hence to sidebands (Bessel bands) around the main resonance frequency. These *sidebands* are equally distanced from the resonant frequency by multiples of the synchrotron tune Q_s. To distinguish the main resonance from its sidebands Q_s is varied.

The synchrotron tune Q_s and the RF voltage are related by [17]:

$$Q_s{}^2 \propto V_{RF} \tag{53}$$

Sidebands are identified by a change of the *RF voltage* which results in a change of synchrotron tune thus changing the distance between resonance dip and its sidebands noticeably. If the sweep is repeated with changed RF voltage one dip stays unchanged and the others are shifted. The unshifted resonance is the main resonance, the shifted resonances are sidebands.

4 Development of Experimental Tools

4.1 Data Acquisition and Real-Time Analysis

The quantities needed to carry out measurements (equations 45, 46) consist of the beam current and the beam lifetime together with a time stamp belonging to each of these values. The SLS control system provides such information by feeding these quantities to EPICS channels which can be read out and remotely archived. It is however necessary to collect this data, save it and evaluate it in *real-time*, in order to adapt the experimental procedure to current circumstances as well as to get experimental results during data acquisition.

An online tool has been provided which reads the data from the EPICS channels, transforms it to an appropriate format and units and then calculates other relevant properties. An example for such a calculation is determining the fraction of beam loss due to elastic gas scattering opposed to the loss through Touschek Scattering at a certain vacuum pressure. This ratio could be derived from the beam current. Recall equation 48:

$$\tau_{ts} = \frac{\tau \cdot \tau_{el}}{\tau_{el} - \tau} \tag{54}$$

and according to [14]

$$\tau_{el}\ [h] = (112 \pm 10) \cdot \frac{(3.2 \pm 0.4)\ [pbar \cdot s]}{P\ [pbar]} \tag{55}$$

with the gas pressure related linearly to the current[8]:

$$P\ [pbar] = 5.11\ [pbar] + 0.01566\ [pbar \cdot mA^{-1}] \cdot I_{beam}\ [mA] \tag{56}$$

Once the necessary values are computed, they are written to a data file for off-line analysis and backup purposes. After a sufficient amount of data has been obtained, certain values of interest can be determined by fitting theoretical models to data. An example of this procedure is the calculation of the current polarization level which requires a polarization build-up to be fitted as depicted in figure 6:

[8] The mentioned linearity is valid in the area of 50-150 mA beam current where our experiments take place, see [14].

$$a + b\left[1 - \exp\left(-\frac{x-c}{d}\right)\right] \tag{57}$$

The important fit parameter is d, the characteristic equilibrium build-up time. In the fit seen in figure 6 $d = 1261 \pm 12$ which (according to equation 41) leads to $\tau_d = (3894 \pm 114)$ s and therefore to $P_{eff} = (62.5 \pm 0.6)$ %.

All these steps were implemented in a single program which allowed a complete online data analysis of polarization build-up in real-time. The actual program code is not complicated, but proved to be a very powerful tool during data acquisition.

4.2 Frequency Sweeping

First measurements of the resonant depolarization frequency were done *by hand*, i.e. the signal generator fed a sine wave signal to the amplifier of a kicker magnet whereby the parameters (sweep range, sweep velocity, gain, etc.) of the signal generator had to be set at the machine manually and the crucial time values (determining the current sweep frequency) had to be noted as well.

In order to get around this tedious and not very accurate method a program has been introduced which allows to control the experiment from the control room with much higher accuracy. The program queries the necessary parameters, writes them to EPICS channels (which can be logged) and, upon start, sends a trigger signal to the signal generator which, on receiving this signal, begins the sweeping of a previously defined range. While sweeping the program writes the actual sweep frequency to an EPICS channel which is written to the same data output files as the measured values (beam current, lifetime, etc.) and therefore enables precise linking between measured values and current experimental parameters.

An example of this procedure is the determination of the resonant depolarizing frequency. When a dip in lifetime is observed, the data is queried for the sweep frequency set on the signal generator during depolarization. This allows precise identification of resonant frequencies as well as measurement of the resonance width. Figure 9 shows an example for the correlation of sweep frequency and depolarization of the beam. When the dip in lifetime occurs (second curve from top) or the rise of losses starts (bottom curve) the current sweep frequency is identified to be the depolarizing frequency. Because the width of this dip (for more detail see chapter 5) is much wider

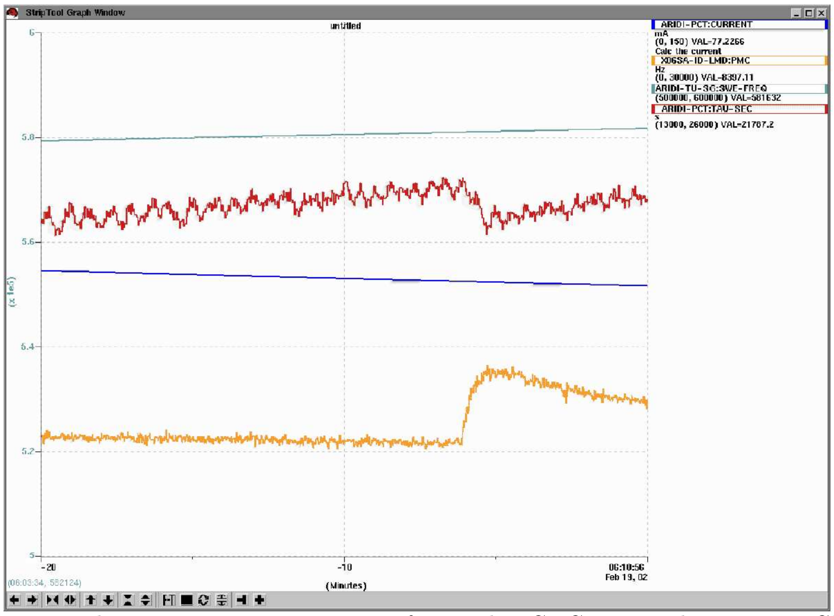

Figure 9: *The experiment as seen from the SLS control system. Shortly before 6:05 the resonant depolarization frequency is reached. The top curve shows the current excitation frequency during the sweep allowing the begin of the dip to be localized at 581,25 kHz.*

than the precision of the sweep frequency, the width of the depolarization dip is the dominating contribution to the resonance uncertainty.

Figure 10 shows the expert panel (provided by the SLS controls group) for setting frequency generator values within the SLS control system.

4.3 Adjusting the RF

Once a dip in lifetime has been observed the next step is to make sure that the dip is the "real" depolarizing resonance and not a sideband or a mirror (see chapters 3.4 and 3.5). Identifying the mirror is simple, because the RF main frequency can easily be changed as mentioned earlier; distinguishing the main resonance from its sidebands however is a bit more difficult because of the fact that the voltages of *all* four RF stations should be changed synchronously (and by well defined means) by a small value in order to change the total RF voltage by as little as necessary. The RF voltage of each RF station can be changed through the SLS control system; normally this is done by hand, one station after the other, but such a procedure is by no means synchronous.

Therefore another computer program was introduced which accomplishes the

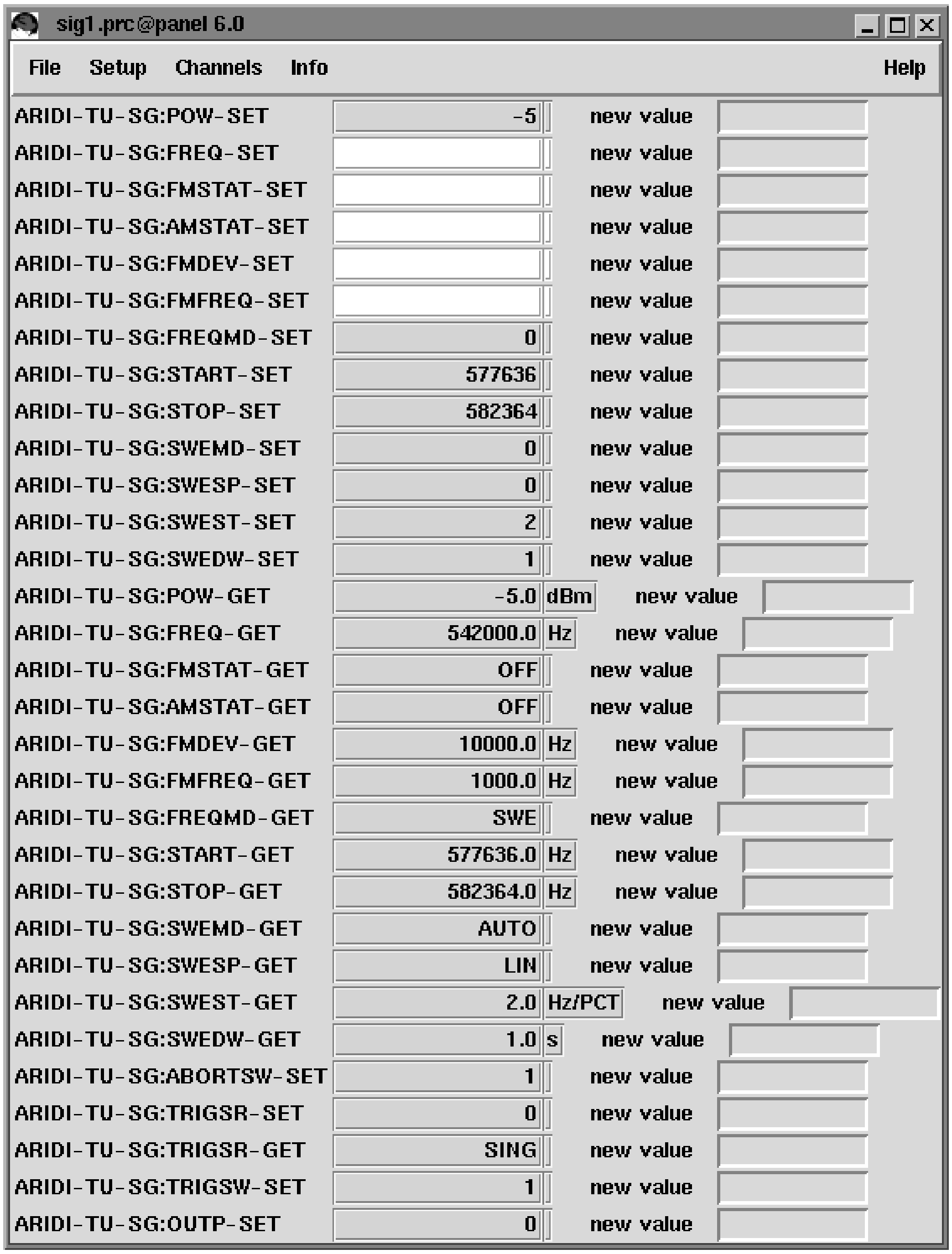

Figure 10: *The panel to set sweep frequency parameters from the SLS control room.*

following tasks: In a first step it acquires the current set voltages of each RF station by querying the corresponding EPICS channels. It then calculates new values depending on a common scaling factor fed to the program as parameter. These new values are then written to the appropriate EPICS channels simultaneously, thus allowing shifts in total RF voltage by well defined means.

5 Measurement Results

In this chapter measurement results will be presented. On nine dedicated shifts polarization experiments have been performed resulting in 23 runs. Not all runs resulted in reasonable data. It was observed that very stable beam conditions were needed in order to guarantee good measurements and that small perturbations (like the closing of a gap by a few mm which leads to additional aperture and thus to a decrease in lifetime) could render a run useless. In the first section results of the polarization build-up measurements are presented, while the second section deals with the energy calibration measurements.

5.1 Beam Polarization Level

The equilibrium beam polarization level was measured as described in chapter 3.2. 90 buckets were filled with a current of ≈ 100 mA. Injection was turned off and an orbit correction was performed to assure that the beam was on the reference orbit. After this correction tune and injection kickers were turned off and the current decay was observed for 30 min to 1 h. As soon as the product of Touschek lifetime and beam current started to saturate the fit of the build-up converged nicely and fit parameters could be derived.

In order to see polarization build-up the tunes first had to be adjusted; $\nu_x = .42$ was much too close to the expected spin tune $\nu = .4465$ so that the beam was expected to polarize only to low levels. Indeed, the polarization build-up was not noticed in a first experiment at this tune setting. The tunes were set back to "old" values used before injection optimization in December. $\nu_x = .42 \rightarrow .38$ and $\nu_y = .19 \rightarrow .16$. As soon as these new tune settings were applied polarization build-up was observed. Figure 11 shows an example of build-up to $(60.1 \pm 0.3)\%$. The two dips in Figure 11 are orbit corrections that were performed during the build-up measurement and led to perturbations of the beam.

In order to reach higher values of polarization another run was performed with a differently corrected orbit and with vertical corrector settings for a flat orbit. This build-up is shown in figure 12; the fit shows polarization build-up of $(86.7 \pm 0.3)\%$.

The build-up measurements show that equilibrium polarization levels close to the Sokolov-Ternov level can be reached. This is in good agreement with the assumption that the depolarizing effects in the SLS storage ring are small.

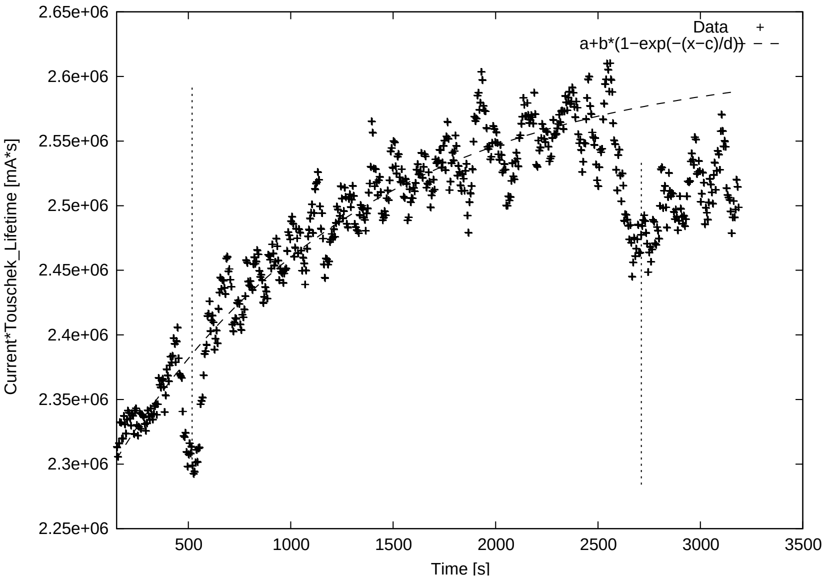

Figure 11: *Polarization build-up and fit (reference orbit with temperature and insertion device bumps). The fit parameter for the characteristic build-up time is* 1213 ± 6 *corresponding to an equilibrium polarization of roughly 60%. The two dips originate from perturbations to the beam induced by orbit corrections.*

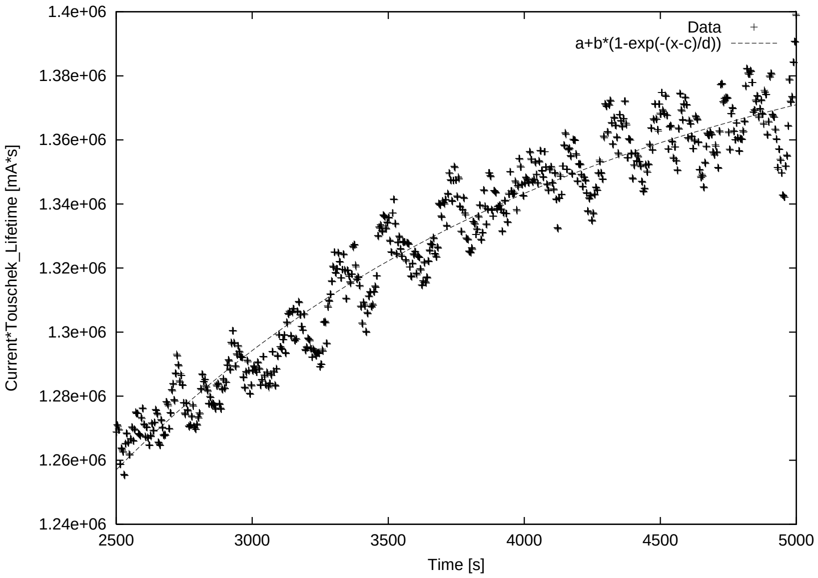

Figure 12: *Polarization build-up and fit (flat orbit). The fit parameter for the characteristic build-up time is* 1751 ± 6 *corresponding to an equilibrium polarization of roughly 87%.*

The verification of high polarization levels in the SLS storage ring is crucial for the following energy calibration measurements. Only high polarization levels of the beam allow noticeable depolarization which leads to significant changes in the Touschek scattering rate and therefore to noticeable signals. For the energy calibration measurements a decent polarization build-up always has to be observed in advance. Once such a build-up has occurred the outcome of the depolarization measurement becomes significant for energy measurement.

5.2 Beam Energy

In order to perform the energy calibration measurement a decent polarization build-up had to be observed as mentioned in the last chapter. Afterwards an orbit correction was done to ensure that the orbit had zero deviation from the design orbit thus the measurement would reveal the actual beam energy not including possible distortion due to corrector settings modifying the integrated bending field. Then the sweep could start within the predefined range and dwell settings. Beam current, lifetime, loss monitor reading and actual sweep frequency were monitored as shown in figure 9.

In a first measurement run we performed a frequency sweep from 2.38 GeV (417.833 kHz) to 2.4 GeV (465.112 kHz) with a dwell of 10 Hz/s and a kicker power of 135 W. The product of beam current and lifetime was flat, thus showing that the resonant frequency had not been reached in this sweep. We decided to start another sweep above 2.4 GeV.

In the second measurement the sweep went from 2.4 GeV (465.112 kHz) to 2.42 GeV (512.391 kHz) with the same power and dwell settings. The result of this run is shown in figure 13. Two effects were observed: At time stamp ≈ 62800 s a dip in the product of beam current and lifetime is noticed due to a lifetime drop by $\approx 5\%$. This dip is located at (490 ± 1) kHz which corresponds to (2.4105 ± 0.0005) GeV, but due to the mirror uncertainty (as already mentioned in chapter 3.4), could also be (2.4366 ± 0.0005) GeV. In a second measurement this dip was reproduced, but due to a vacuum interlock the identification of the mirror had to be postponed. The second important effect seen in figure 13 are the three peaks; the central peak is a (not yet identified) orbital resonance with two sidebands. The sidebands are located at ± 6.4 kHz from the center resonance which corresponds to a synchrotron tune of $Q_s \simeq 6.12 \cdot 10^{-3}$. An interesting fact is that to the right of the the depolarizing dip the plotted curve isn't flat as one would expect from the resonance crossing formula of Froissart and Stora [18]: After the

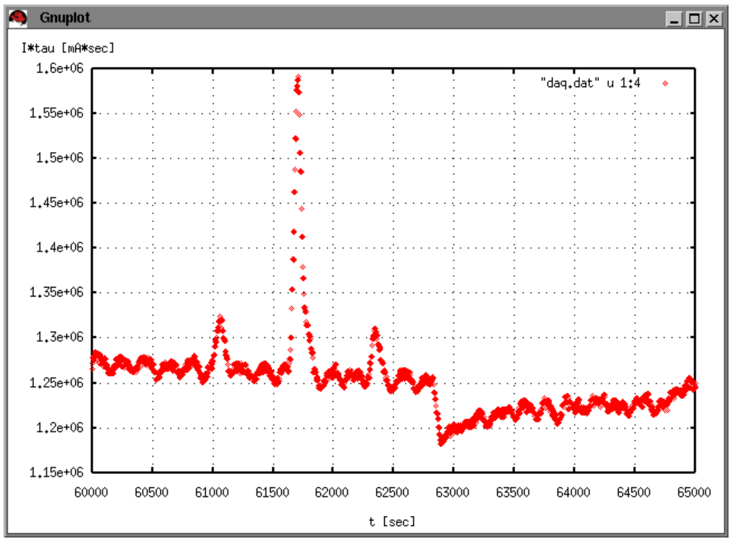

Figure 13: *First sweep around a depolarizing resonance. The resonance is located at 62800 s whereas the three peaks come from an orbital resonance; a central resonance and its first order sidebands. The distance between center resonance and sidebands is the synchrotron tune.*

resonance dip a new build-up is observed with the same exponential build-up characteristics as observed in equilibrium polarization level measurements (see also figure 19).

In a third run we tried to reproduce the dip above the half number (the half number spin tune corresponds to 520.833 kHz). The sweep went from 523 kHz to 591 kHz with a dwell of 18 Hz/s and 250 W kicker power. The result is shown in figure 14. A clear dip shows that the depolarizing resonance lies at (580.0 ± 0.2) kHz corresponding to (2.4486 ± 0.0001) GeV or the mirror at (2.3985 ± 0.0001) GeV. This dip is confirmed in the peak of loss monitor coincidence signals as depicted in figure 15. It was however observed at the end of the sweep that the mean orbit had drifted, thus causing the energy to change. Therefore the measurement had to be repeated.

In a fourth run the last measurement was verified: In a fast sweep (dwell was 30 Hz/s) from 523 kHz to 607 kHz a pattern of dips was detected starting at (547.0 ± 0.5) kHz. This is shown in figure 16. A second dip is at (552.9 ± 0.5) kHz and a third at (558.6 ± 0.5) kHz; afterwards the orbit resonance leads to the three peaks already seen in earlier experiments - they are again separated by the synchrotron tune. Note that the orbit resonance peaks are to the right of the depolarizing resonance compared to figure 13 where they were to the left. This has to do with the fact that we are now sweeping above

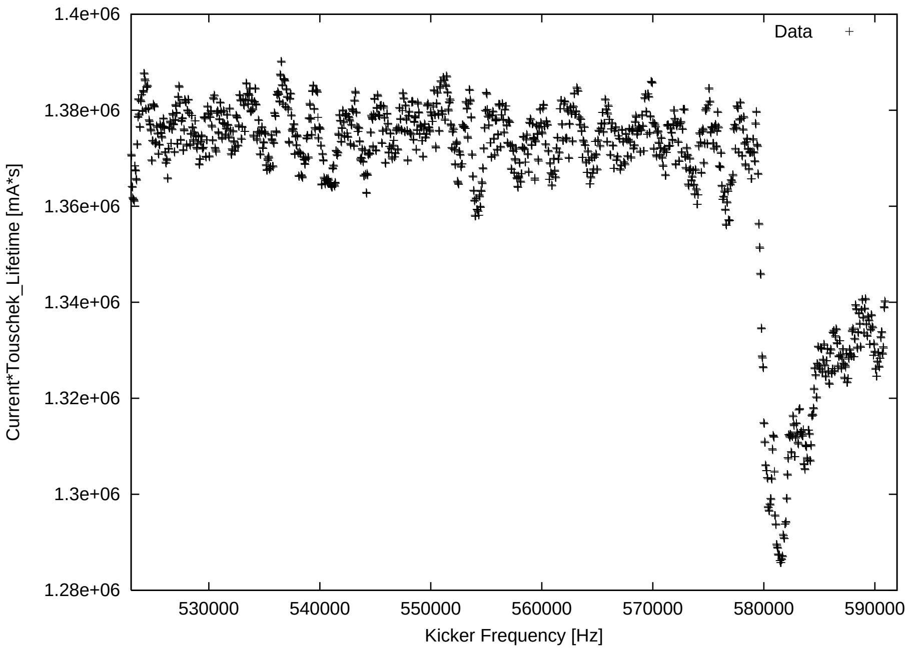

Figure 14: *The depolarizing resonance at 580kHz.*

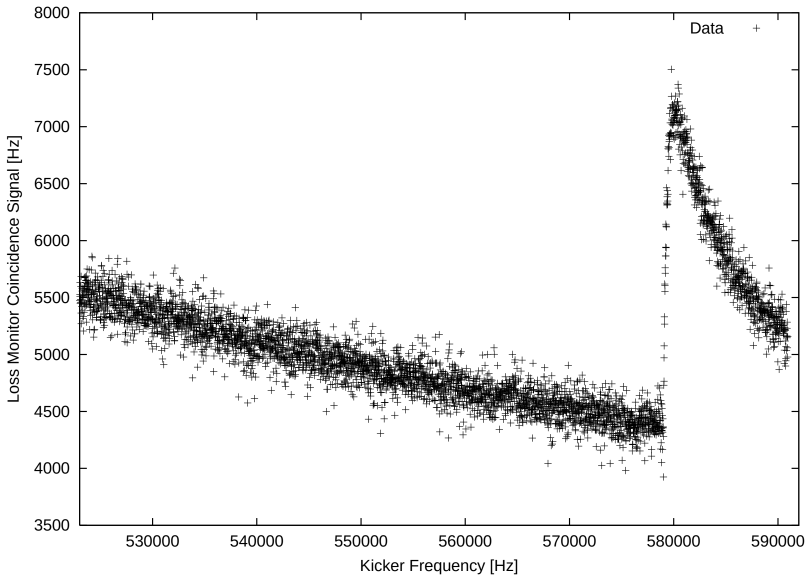

Figure 15: *The loss monitor coincidence signal rising during resonant depolarization at 580kHz.*

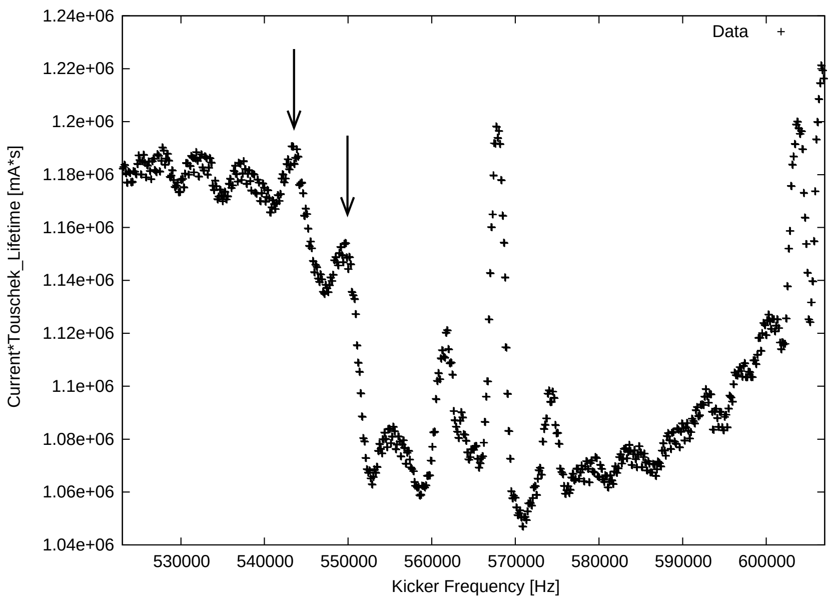

Figure 16: *Dip pattern of a fast sweep.*

the half-integer so our view is "mirrored".

The three dips correspond to the energies (2.434 ± 0.002) GeV (mirror at (2.413 ± 0.002) GeV), (2.437 ± 0.002) GeV (mirror at (2.410 ± 0.002) GeV) and (2.440 ± 0.002) GeV (mirror at (2.408 ± 0.002) GeV). The question arises which of these dips is the resonance and which are sidebands as well as is this the resonance or just its mirror? To answer these questions two identical runs were started differing only by a changed RF voltage. Prior to the second sweep the RF voltages were increased from 1752.1 kV to 1944.8 kV (+11%). According to equation 53 this should lead to a change of the synchrotron tune Q_s by more than a percent which can be observed easily. The patterns of the two sweeps are compared in figure 17.

The synchrotron tune increased by $\approx 5\%$ and one dip could be identified to have not moved within the precision of measurement. Another dip (to the left of the resonance) was shifted by 5% to lower frequencies while a dip above the resonance was shifted to higher frequencies, precisely as predicted by theory. The resonance is located at (550.4 ± 0.6) kHz corresponding to (2.4361 ± 0.00024) GeV (mirror at (2.4110 ± 0.00024) GeV).

A magnified view of the resonance dip is given in figure 18. Notice the fit curve from the upper level (polarized beam) to the lower level (partially depolarized beam) according to the Froissart-Stora equation [18]. Froissart and Stora described the curve that would be observed when crossing a depolar-

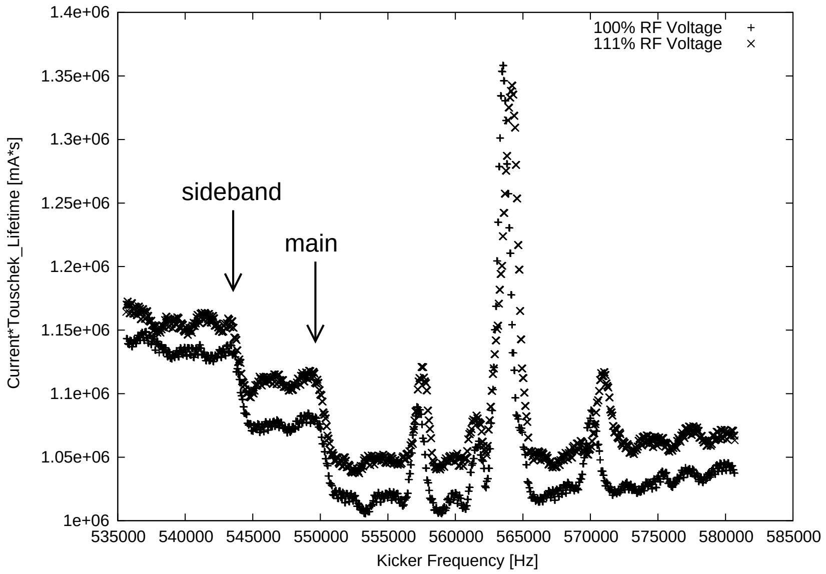

Figure 17: *Dip patterns of two sweeps differing by a slightly changed RF voltage.*

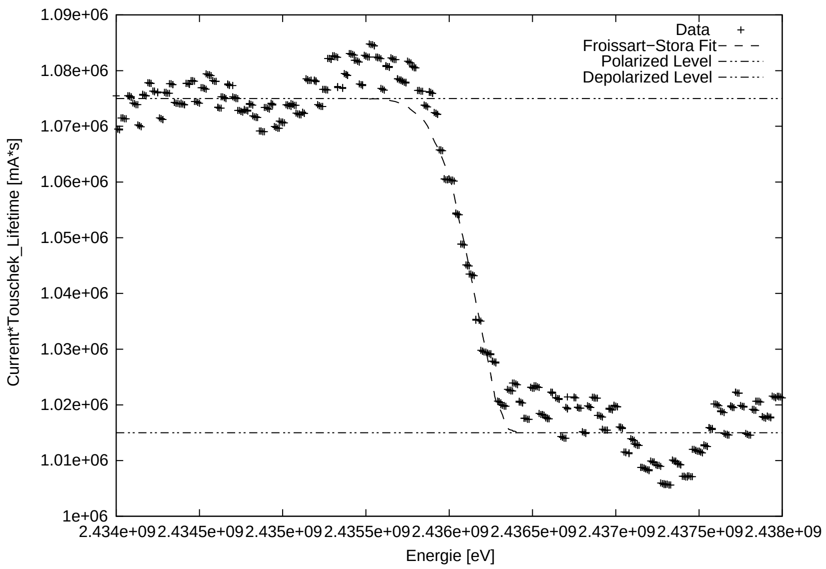

Figure 18: *Dip of the resonance with fit according to the Froissart-Stora equation for resonance-crossing.*

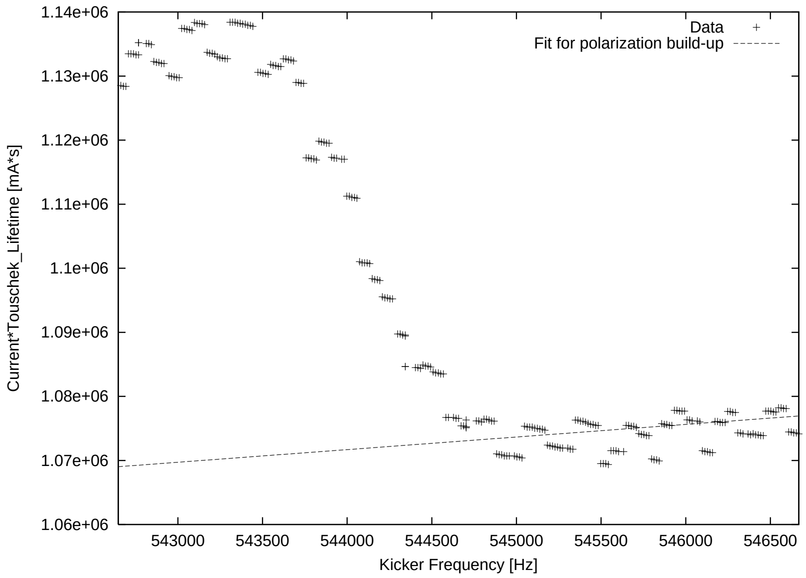

Figure 19: *Slow polarization build-up process after having crossed the depolarizing resonance.*

izing resonance and claimed it to be:

$$\frac{P_{pol}}{P_{depol}} \propto 2\exp(-\frac{\pi\epsilon^2}{2\alpha}) - 1 \tag{58}$$

where ϵ is the strength of the resonance and α the resonance crossing speed. The slow build-up after crossing the resonance is due to the fact that the kicker magnet has already depolarized a large fraction of the beam while being in the area of the resonance. When the sweep reaches values outside of the resonance a slow polarization build-up starts again thus leading to a almost flat curve. A very nice example for this build-up process after crossing the depolarizing resonance is shown in figure 19.

The exact energy calibration is obtained with the Froissart-Stora fit: The energy is the minimum of the Froissart-Stora dip minus half of the FWHM of the Froissart-Stora fit. The uncertainty of the dip is independent of the signal generator driving the sweep as already mentioned in chapter 3.3. Therefore we specify the energy uncertainty with the half-FWHM of the Froissart-Stora fit. Applied to the data and fit seen in figure 18 this leads to an energy of (2.4361 ± 0.00024) GeV (mirror at (2.411 ± 0.00024) GeV) where the 240 keV uncertainty correspond to the 480 keV FWHM of the Froissart-Stora fit. The distinction between resonance and mirror could not be done, because the

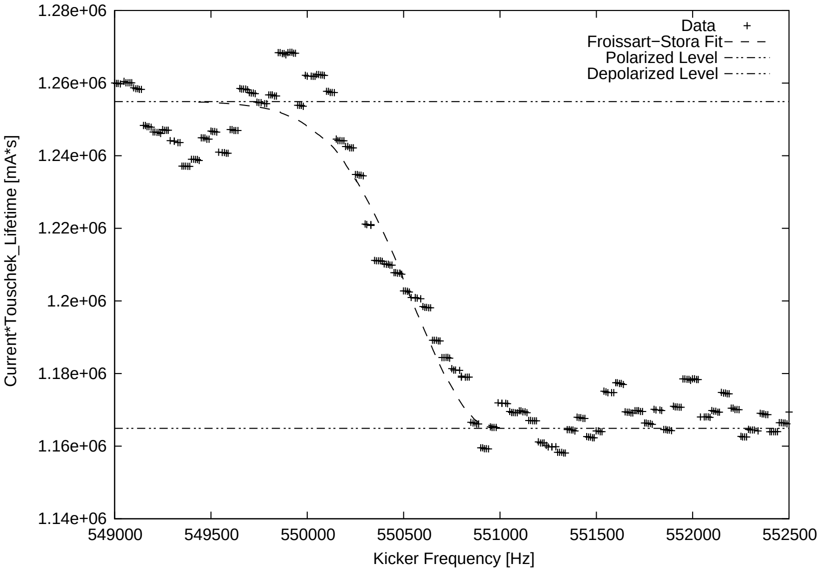

Figure 20: *Froissart-Stora fit of the depolarizing resonance.*

beam was dumped due to a shutter interlock shortly before the end of shift.

A week later this run was repeated but we planned to reduce dwell and kicker strength in order to receive a more narrow dip, thus increasing certainty of the energy calibration. After observing build-up and correcting the orbit a sweep from 536 kHz to 579 kHz was carried out. When the orbit had been checked to have no deviation form the flat orbit we noted the RF main frequency to be at $\nu_{RF} = 499654310$ Hz. The resonance dip was found at (2.4361 ± 0.00018) GeV (mirror at: (2.411 ± 0.00018) GeV) as shown in figure 20.

In a second step the RF main frequency was changed by +1000 Hz to $\nu_{RF} =$ 499655310 Hz. Now the orbit had larger mean values in the arcs in agreement with theory. According to the orbit correction program of the SLS control system (see equation 52) $\Delta\nu_{RF} = +1$ kHz leads to an energy deviation of $\Delta E \approx -7$ MeV. But actually the reproduced dip was now found 7 MeV *above* the original 2.4361 GeV. This proves that 2.4361 GeV is the actual resonance and not the mirror; the mirror of this resonance would be seen if sweeping around the mirror frequency of 491 kHz. The reason for this conclusion lies in the fact that 2.4361 GeV already lies above the half-integer spin tune (520.8 kHz or 2.4236 GeV), so in the sweeps around this frequency we have been looking at mirror frequencies. If the energy belonging to the shifted RF voltage lies higher even though it should be lower than the energy belonging to the unshifted RF voltage, we are looking at the mirror of a mirror, i.e.

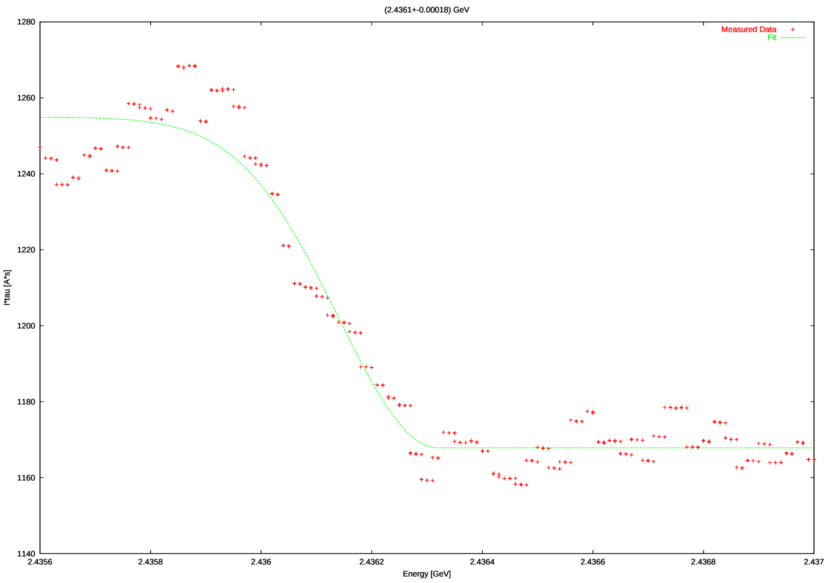

Figure 21: *The depolarizing resonance dip corresponding to a beam energy of* (2.4361 ± 0.00018) *GeV.*

we are looking at the actual resonance! Therefore we will from now on link all resonances in sweeps from frequencies above the half-integer to energies above 2.4236 GeV. Figure 21 shows the result of these two runs.

In the last run we planned to reproduce the results of the previous runs but with higher accuracy. We therefore lower the kicker power from 250 W to 50 W and set the dwell to only 2 Hz/s. We were able to reproduce the resonance but at a much higher energy of (2.4490 ± 0.00011) GeV as shown in figure 22.

The reason for this sudden "energy drift" however has nothing to do with the actual beam energy as we were able to show later. During the measurement the only peculiarity observed was an exceptionally low RF main frequency of 499653209 Hz; this value was about 1 kHz lower than in previous runs. After carefully studying the events of this night shift it was recognized that the orbit was flat and centered, but that there was a mean corrector setting leading to an orbit which was too far inside of the ring with respect to the design center. Because there was a systematic shift to smaller radii, the RF main frequency was lowered by the orbit correction to smaller values, thus increasing the actual beam energy. It is important to notice that not only does the beam have to be on the reference orbit for the energy calibration to render decent values, but also the correctors pattern is not allowed to have

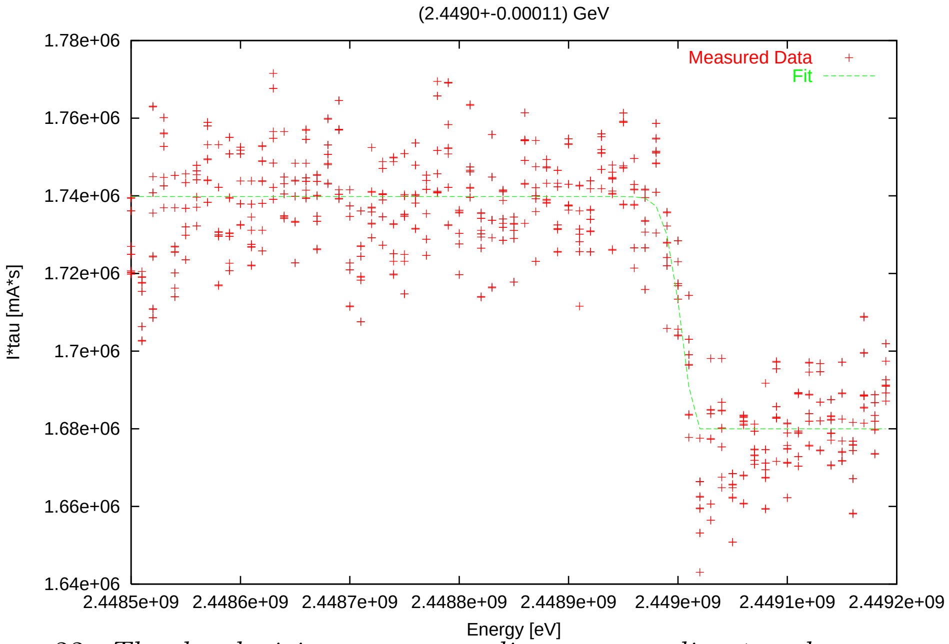

Figure 22: *The depolarizing resonance dip corresponding to a beam energy of* (2.4490 ± 0.00011) *GeV.*

a mean value in the dispersive regions (in the arcs). If the mean corrector value is zero the orbit is centered with respect to the design orbit and energy calibration measurements lead to valid results. In other cases the orbit correction will start shifting the RF main frequency and thus will shift the beam energy.

Notice however that the uncertainty of the last run is already as low as $\frac{\Delta E}{E} = 4.5 \cdot 10^{-5}$ meaning that the precision of the energy calibration measurement can be increased with the lower kicker power and dwell settings as described above. Further runs are expected to reach a precision of $\frac{\Delta E}{E} = 10^{-5}$!

Finally, we have measured the energy of the SLS storage ring to be (2.4361 ± 0.00018) GeV and its stability over a couple of weeks is constant within $\frac{\Delta E}{E} = 4.5 \cdot 10^{-5}$. This is in good agreement with independent energy calibration measurements performed by experimenters in one of the SLS beam lines [19]; by looking at characteristic line spectra behind undulator U24 (gap at 8 mm) the energy was calibrated at (2.44 ± 0.02) GeV which is in excellent agreement to the presented measurements.

6 Outlook

The carried out experiments have allowed to measure the SLS storage ring beam energy with very high precision. They have however also shown how tedious and time consuming this method is. It is also very sensitive to perturbations of all kind including gap size changes, tune shifts and orbit drifts. Therefore this method is not a priori suitable for day-to-day parasitic measurements in order to monitor the current beam energy.

Nevertheless it is possible that in the future when SLS operates without frequent shutdown periods and therefore acquires an immanent stability this measurement could be carried out in a short time frame between user shifts allowing an independent check of the beam energy. Such measurements could be used to perform studies on beam stability during typical beam lifetimes and beam drifts during longer run periods. In the long term these studies could help better understanding properties of the SLS storage ring.

Today the high precision of the energy calibration method already allows for a more precise calculation of the momentum compaction factor and its non-linearity (equation 52). Up to now all calculations of this non-linearity were restricted by the precision of the beam energy. In addition the performed energy measurements have shown that the maximum precision has not yet been reached. By lowering the kicker strength and the sweep dwell the depolarizing resonance can be made sharper, thus leading to less uncertainty of the energy calibration. It is expected that future applications of this measurement method at SLS will lead to knowledge of beam energy with a precision of $\frac{\Delta E}{E} = 10^{-5}$. Such uncertainties are much smaller than those obtained by measurement of the dipole magnet fields with Hall probes.

Another suggested consequence of these energy measurements is to investigate if the injection from booster to storage ring can be enhanced by matching the energies of the two rings. It has been mentioned that possibly a mismatch between booster and storage ring energy is limiting the injection rates. If the booster injects at design energy and the stored beam in the storage ring has an energy that lies over one percent higher, this could in fact cause injection efficiency to suffer. Investigation of this problem will follow soon.

Apart from the suggested experiments to follow this calibration the original problem has to be solved as well: Why is the beam energy in the SLS storage ring so much higher than the design energy? The currents measured during dipole field measurements are in agreement with the magnet calibration. This leads to the presumption that the dipole magnet measurements have rendered wrong calibration constants between applied current and generated magnetic field for a given hysteresis cycle. As a consequence the dipole fields will be measured again with Hall probes in the near future.

7 Acknowledgements

I would like to thank Prof. Dr. Ralph Eichler for giving me the opportunity to do these studies and work at the Swiss Light Source.

Many thanks go to my supervisors Dres. Lenny Rivkin and Michael Böge who helped me so much during these last four months. I appreciated their kind and motivating suggestions as well as their questions and criticism. I could always count on their support which has been very helpful for me in order to conclude this thesis.

I would also like to thank Dres. Andreas Streun, Marc Muñoz, Micha Dehler, Miroslav Dach, Thomas Schmidt, Werner Portmann and Andreas Lüdeke for their advice and helpful explanations. My thanks also go to Peter Hottinger, Andreas Jaggi and Dr. Trivan Pal for their support of my experiments during our night shifts.

Finally many thanks to the whole team at SLS for a terrific time at their lab, for the good working climate and all those great moments. This has been a very interesting and fun experience and I will always gladly look back on this period of my graduate studies at ETH.

References

[1] L. Rivkin: private conversation about preliminary material

[2] Y. S. Derbenev et al.: *Accurate Calibration of the Beam Energy in a Storage Ring Based on Measurement of Spin Precession Frequency of Polarized Particles*, Particle Accelerators, 10, 1980

[3] F. Frommberger: *Energiekalibration bei ELSA*, `http://elsahp7.physik.uni-bonn.de/Forschungsgebiete/Strahldiagnose/Energiekalibration/Energiekalibration.html`, July 2001

[4] P. Kuske et al.: *High Precision Determination of the Energy at BESSY II*, Proceedings of EPAC 2000, Vienna, Austria

[5] C. Steier et al.: *Energy Calibration of the Electron Beam of the ALS Using Resonant Depolarization*, Proceedings of EPAC 2000, Vienna, Austria

[6] A. W. Chow: *Polarization of a Stored Beam*, Lecture given at the 1981 Summer School on High Energy Particle Accelerators, Fermi National Accelerator Laboratory

[7] R. Schmidt: *Polarisationsberechnungen am Speicherring PETRA*, Thesis, University of Hamburg/DESY, 1982

[8] A. A. Sokolov, I. N. Ternov: *On Polarization and Spin Effects in the Theory of Synchrotron Radiation*, Sov. Phys. Doklady 8, 1203 (1964)

[9] V. Bargman, L. Michel, V. L. Telegdi: *Precession of the Polarization of Particles Moving in a Homogeneous Electromagnetic Field*, Phys. Rev. Lett. 2, 435 (1959)

[10] M. Böge: *Analysis of Spin Depolarizing Effects in Electron Storage Rings*, DESY Report 94-087, May 1994

[11] R. Neumann, R. Rossmanith: *A Fast Depolarizer for Large Electron-Positron Storage Rings*, Nucl. Inst. Meth. 204, 29 (1982)

[12] M. Böge: *The Status of Polarization Studies at HERA*, Talk given for the HERA Polarization Group, DESY, January 1993

[13] R. Neumann: *Depolarisation des Strahls am Speicherring PETRA mit Hilfe von zeitabhängigen Magnetfeldern*, Diplomarbeit, Universität Hamburg, 1981

[14] A. Streun: *First Lifetime Evaluation for SLS*, Preliminary Paper, November 2001

[15] S. Khan: *Simulation of the Touschek Effect for BESSY II*, Proceedings of EPAC 1994, London, England

[16] W. T. Ford, A. K. Mann, T. Y. Ling: *Beam Polarization Effects in High Energy Electron-Positron Storage Rings*, SLAC Report No. 158, November 1972

[17] H. Wiedemann: *Particle Accelerator Physics I*, Second Edition, Springer Verlag

[18] M. Froissart, R. Stora: *Dépolarisation d'un faisceau de protons polarisés dans un synchrotron*, Nucl. Inst. Meth. 7, 297 (1960)

[19] C. Schulze-Briese, preliminary material and private conversation